JOURNAL OF GUIDANCE, CONTROL, AND DYNAMICS
Vol. 34, No. 2, March–April 2011

Engineering Notes

Evolution of Periodic Orbits in the Sun–Mars System

Pooja Dutt* and R. K. Sharma†
Vikram Sarabhai Space Center, Thiruvananthapuram 695022, India

DOI: 10.2514/1.51101

I. Introduction

THE backbone of analysis in most dynamic systems is the study of periodic motions, since they greatly assist in understanding the structure of all possible motions. Recently Dutt and Sharma [1] analyzed the Poincaré surface of sections for the Earth–Moon system and identified periodic, quasi-periodic orbits and chaotic regions.

As the classical model of the restricted three-body problem does not account for some of the perturbing forces such as oblateness, radiation pressure and variations of the masses of the primaries, researchers have included these forces in the study of the restricted three-body problem. In 1891 Lebedev experimentally demonstrated the minute pressure exerted by light on bodies and stated a law according to which this pressure is inversely proportional to the square of the distance between the light source and the illuminated body. Since then, researchers have taken into consideration this force as well, apart from other perturbing forces. Yarkovski (around 1900), Poynting [2] and Robertson [3] showed that the role of the radiation force is rather complicated and the effects it produces on the dynamics of the small body depend on its particular geometry, physical and physicochemical characteristics. In 1950, Radzievskii [4] proposed a simplified theory, trying to facilitate the investigation of similar problems without altering the fundamental character of the system. Since then some of the notable research in the photo-gravitational restricted three-body problem are by Chernikov [5], Manju and Choudhry [6], Kumar and Choudhary [7], Lukyanov [8], Kalvouridis et al. [9], Sharma [10,11], Sharma and Ishwar [12], Bhatnagar and Chawla [13], Kalantonis et al. [14], Kunitsyn and Perezhogin [15], Kunitsyn and Tureshbaev [16], Papadakis [17], Ragos and Zagouras [18,19], Schuerman [20], Abdul Raheem and Singh [21], Namboodiri et al. [22], Markellos et al. [23], and Das et al. [24,25].

A number of iterative schemes to compute periodic orbits numerically have been used in literature. Some of them are by Szebehely [26], Broucke [27], Markellos [28], Gonczi and Froeschle [29], Cielaszyk and Wie [30], Papadakis [31], Henon [32], Perdios et al. [33], Tsirogiannis et al. [34], Russell [35], Viswanath [36], Deprit and Rom [37], Williams [38], and Guibout and Scheeres [39]. The set of stable periodic and quasi-periodic trajectories define regions of regular motion or stability "islands" that spread in a chaotic "sea" made of trajectories with high sensitivity with respect to the initial conditions. Poincaré maps give a qualitative picture of stability regions in the planar problem. In this Note, a study on periodic orbits in the sun–Mars system using the Poincaré surface of section technique, when the more massive primary (sun) is the source of radiation, has been carried out. The stability evolution of periodic orbits around Mars and the sun are studied. Effect of the radiation pressure on the periodic orbits is also investigated.

Received 9 June 2010; revision received 16 November 2010; accepted for publication 16 November 2010.

*Scientist, Applied Mathematics Division; pooja_dutt@vssc.gov.in.
†Head, Applied Mathematics Division; rk_sharma@vssc.gov.in.

II. Planar Circular Restricted Three-Body Problem

The motion of the spacecraft is simulated by numerically integrating the planar circular restricted three-body problem. This defines the motion of the spacecraft on the plane of motion of the sun and Mars, which are assumed to move in circular motion about their center of mass. We use a coordinate system (x, y), which rotates with unit velocity, where the x-axis is along the sun–Mars line. The coordinates are scaled so that the sun is at the location $(-\mu, 0)$, and the Mars is at $(1-\mu, 0)$, where $\mu = m_2/(m_1 + m_2)$ $(=3.2268352164 \times 10^{-7})$ is the mass ratio and m_1

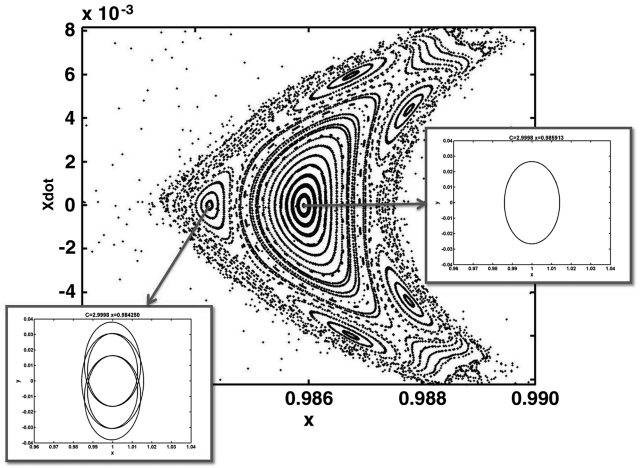

Fig. 1 PSS for Jacobi constant $C = 2.9998$ and periodic orbits lying at the center of the islands.

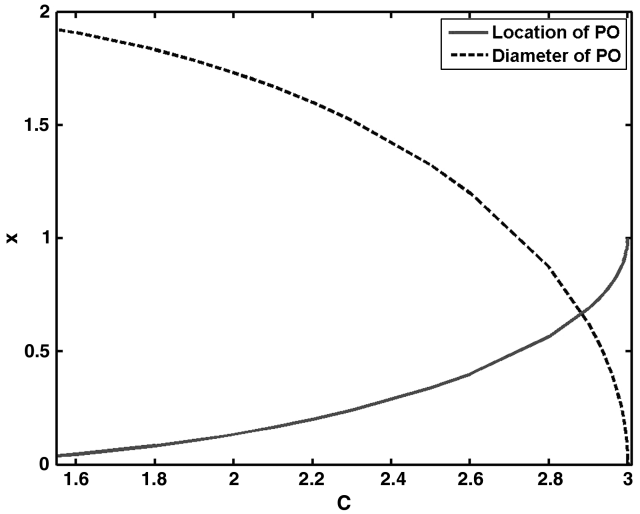

Fig. 2 Location of the center of the KAM tori containing the retrograde Mars-centered periodic orbits (labeled *PO* in all figures) and the diameter of these orbits (the distance between the two points where the periodic orbit intersects sun–Mars line).

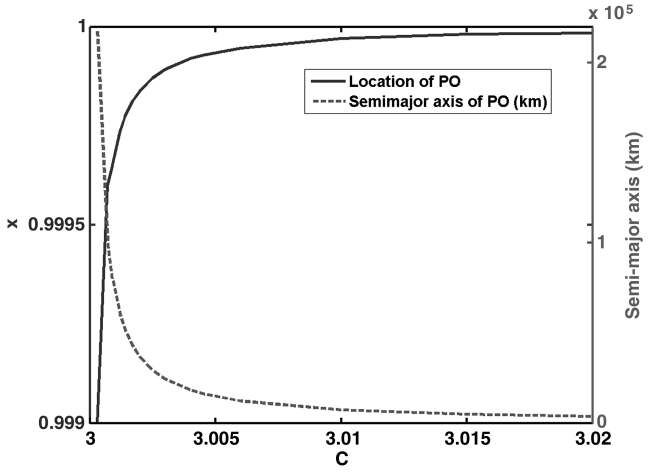

Fig. 3 Location of center of KAM tori and the semimajor axis of Mars-centered periodic orbits for $C = 3.0$ to 3.02.

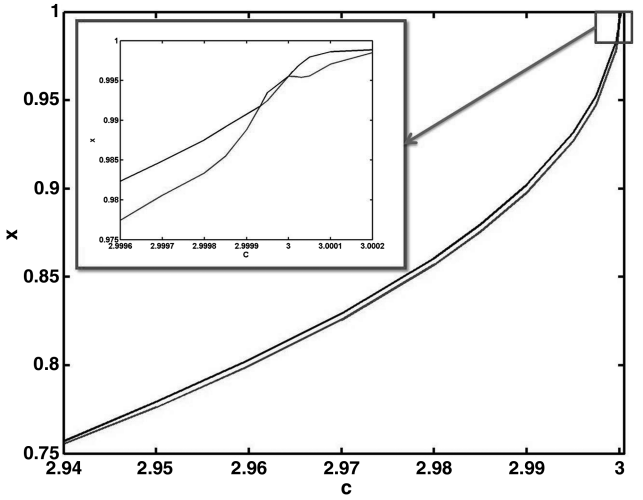

Fig. 5 Size of KAM tori as function of Jacobi constant C. The upper line corresponds to the left most tip and the lower line corresponds to the right most tip of the island obtained by PSS, on the sun–Mars line.

($=1.9891 \times 10^{30}$ kg) and m_2 ($=6.4185 \times 10^{23}$ kg) are the masses of the sun and Mars, respectively.

The radiation force on a particle (spacecraft), exerted by a radiating body, generally consists of three terms, namely the radiation pressure, the Doppler shift of the incident radiation and the Poynting drag (Poynting [2], Robertson [3]). The first two act radially and the third one acts opposite to the velocity vector. The latter two components are caused by the absorption and subsequent reemission of radiation and constitute the Poynting–Robertson effect. Radzievskii [4] made the assumption that this effect is negligible and that the only significant force is radiation pressure.

The effect of radiation pressure of a source on a small particle is expressed by means of the mass reduction factor $q = 1 - \varepsilon$, where the radiation coefficient ε, is the ratio of the force F_p which is caused by radiation to the force F_g which results from gravitation, that is $\varepsilon = F_p/F_g$. This coefficient depends on the physical properties of the radiating body, as well as those of the particle and is expressed by the formula given by

$$\varepsilon = \frac{3L}{16\mu cGM\rho s} \tag{1}$$

where G, M and L are, respectively, the gravitational constant, mass and luminosity of the sun. Luminosity depends on the absolute temperature T of sun (Lukyanov [8]). s and ρ are, respectively, the mass and uniform density of the particle. Knowing the mass and the luminosity of the sun, ε can be evaluated for any particle of a given radius and density.

Solar radiation pressure force F_p changes with distance by the same law as the gravitational attraction force F_g and acts opposite to it. So it is possible to consider that the resulting action of this force will lead to reducing the effective mass of the sun. Thus, sun's resulting force acting on the particle is (Kalvouridis et al. [9])

$$F = F_g - F_p = \left(1 - \frac{F_p}{F_g}\right)F_g = qF_g \tag{2}$$

If $q = 1$, radiation has no effect. If $q < 0$, then radiation surpasses gravity and if $0 < q \leq 1$, gravitational force exceeds radiation. The latter case is the most common. The equations of motion of the spacecraft are (Szebehely [26], Sharma [10,11])

$$\ddot{x} - 2\dot{y} - x = -q(1-\mu)\frac{(x+\mu)}{r_1^3} - \mu\frac{(x-1+\mu)}{r_2^3} \tag{3}$$

$$\ddot{y} + 2\dot{x} - y = -\left[\frac{q(1-\mu)}{r_1^3} + \frac{\mu}{r_2^3}\right]y \tag{4}$$

where $r_1^2 = (x+\mu)^2 + y^2$, $r_2^2 = (x-1+\mu)^2 + y^2$.

Let $Z = (x, y, \dot{x}, \dot{y})$, and $Z(t)$ be a general solution of the differential equations, where t is defined over the interval $[t_1, t_2]$,

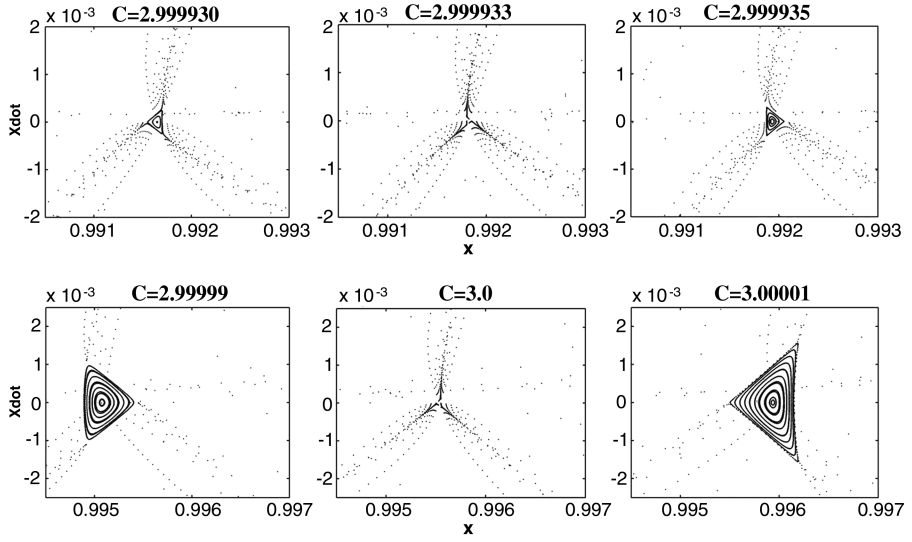

Fig. 4 PSSs near the transitions at $C = 2.999933$ and $C = 3.0$.

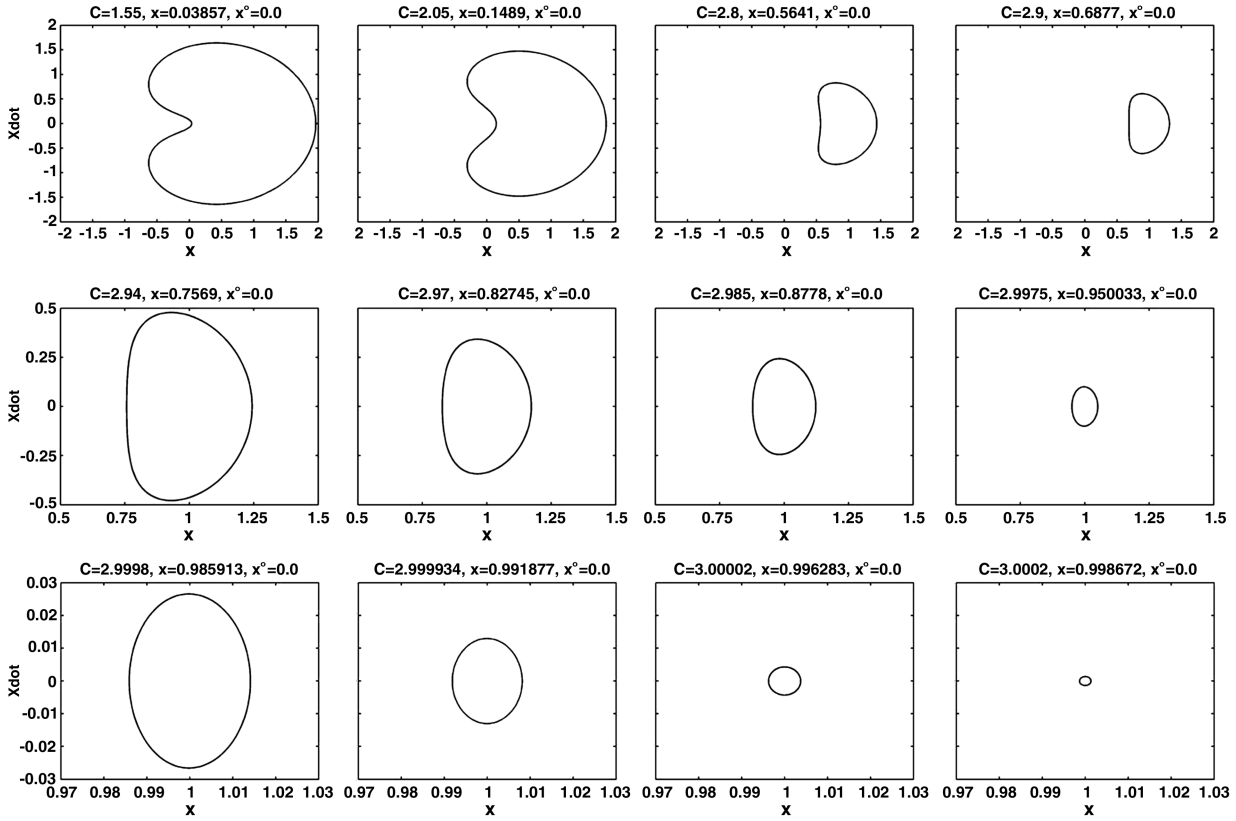

Fig. 6 Mars-centered retrograde periodic orbits (the figures in a row have same scale).

$t_1 < t_2$. Associated with this system is the general energy of the spacecraft, called the Jacobi energy function, which is a constant along the solutions and is called the Jacobi constant C. The motion of spacecraft can be restricted to the surfaces $Q = C$ which are three-dimensional in the four-dimensional phase space Z. The energy E of the orbit corresponds to the energy integral or Jacobi integral:

$$E = -\frac{C}{2} = \frac{1}{2}(\dot{x}^2 + \dot{y}^2) - \frac{1}{2}[(1-\mu)r_1^2 + \mu r_2^2] - q\frac{1-\mu}{r_1} - \frac{\mu}{r_2} \tag{5}$$

To view the dynamics of the spacecraft, we make special two-dimensional slices through Q for different values of C. The two-dimensional section is labeled S and defined as $S = \{y = 0, \dot{y} > 0\}$. These are called Poincaré sections. To make them, thousands of intersections are made with the numerically integrated trajectory of the spacecraft on S, and the resulting points of intersection are recorded. This surface of section technique is used for identification of periodic and quasi-periodic orbits, regular or chaotic nature of the trajectory and the extent of the particle's motion throughout the phase space. Smooth and well-defined islands represent regular motion. Kolmogorov–Arnold–Moser (KAM) theory guarantees the presence of quasi-periodic orbits, which appear as closed curves surrounded by random distribution of points which represent chaotic motion. Periodic orbits appear as isolated single points inside such islands. The regular regions can be interpreted as regions of stability in the sense that outside them the motion is unstable (chaotic) and inside them the motion is in general regular, except for the thin chaotic layer associated to the separatrices of secondary resonances. Thus, the

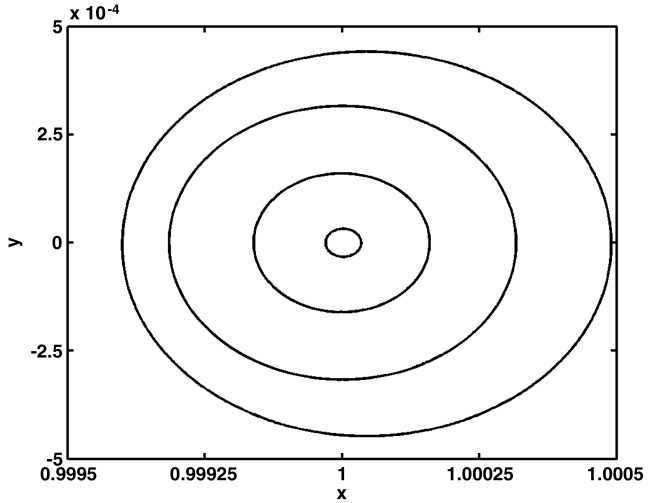

Fig. 7 Mars-centered retrograde periodic orbits for $C = 3.01$, 3.002, 3.001, and 3.0007. The orbit with biggest and smallest diameter corresponds to $C = 3.0007$ and 3.01, respectively.

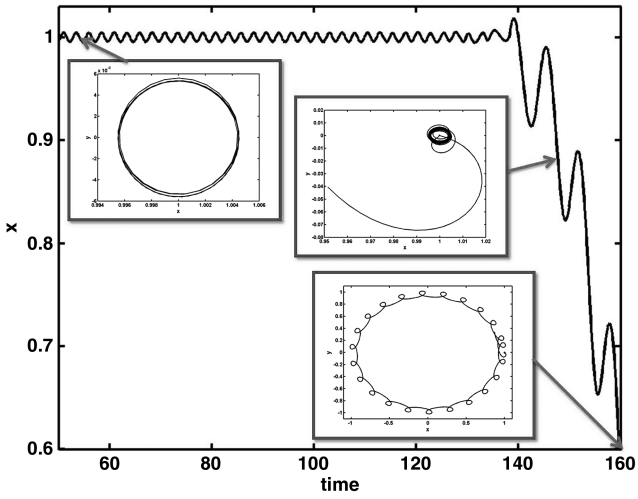

Fig. 8 Trajectory of a particle for $C = 3.0$ and with initial condition $x = 0.9956, \dot{x} = 0$ and snapshots of the orbit at different time instances. A Mars-centered orbit is slowly transformed into a sun-centered orbit.

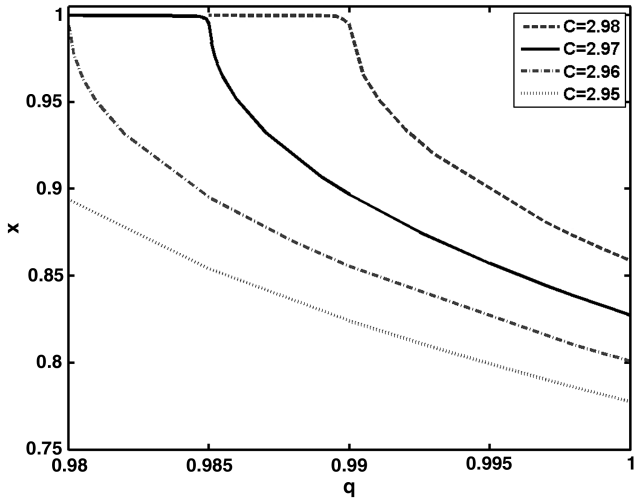

Fig. 9 Location of the center of KAM tori containing the Mars-centered periodic orbits with variation in solar radiation pressure (q).

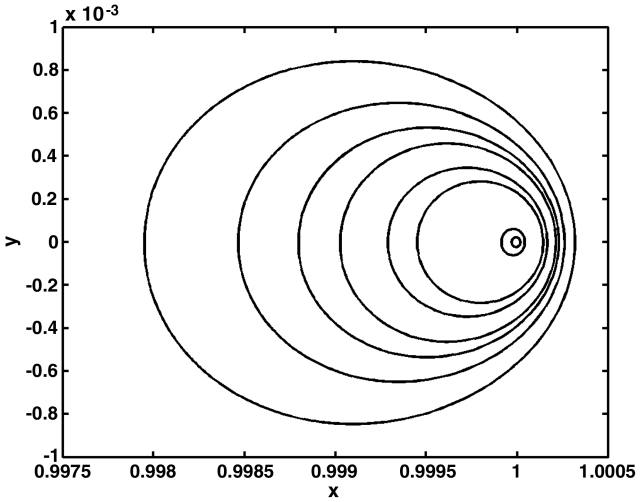

Fig. 11 Mars-centered periodic orbits for Jacobi constant $C = 2.97$ and $q = 0.9849, 0.98485, 0.9848, 0.98475, 0.98465, 0.98455, 0.9825$, and 0.9780. The orbits with biggest and smallest diameter correspond to $C = 0.9849$ and 0.9780, respectively.

maximum amplitude of oscillation, which is the largest of the quasi-periodic orbits (KAM tori) can be taken as a parameter to measure the degree of stability of the periodic orbit with respect to the region around it in the phase space (Winter [40]).

III. Numerical Results

We have explored the sun-centered and Mars-centered orbits in the sun–Mars system and variations in them due to solar radiation pressure.

A. Evolution of Mars-Centered Orbits Without Radiation Pressure

To generate Poincaré surface of sections (PSSs), the initial values of x were selected by taking $y = \dot{x} = 0$ and $\dot{y} > 0$. Depending upon the need, the distance between two consecutive starting conditions Δx and time step size (Δt) was between 10^{-3} to 10^{-6}. These starting conditions were used in numerical integration of the equations of motion, carried out with the fourth-order Runge–Kutta–Gill method.

PSS technique revealed the existence of a family of Mars-centered and a number of sun-centered orbits with respect to C. Mars-centered retrograde periodic orbits exist for C lying between 1.55 and 3.03 and are contained in KAM tori in the PSS which are easily identified in the sea of random points. As an illustration, PSS for $C = 2.9998$, along with two periodic orbits that lie at the center of the islands, have been shown in Fig. 1. As shown in Fig. 2, KAM tori shift towards Mars with the increase in C and orbits with decreasing diameter are obtained. From $C = 3$ to 3.02, the location of KAM tori containing these periodic orbits moves towards Mars and their size decreases significantly (Fig. 3). It is seen that there is transition in oscillations in the KAM tori for C lying between 2.9996 to 3.0002. The width of the KAM torus increases from $C = 2.94$ to 2.9975, where it is

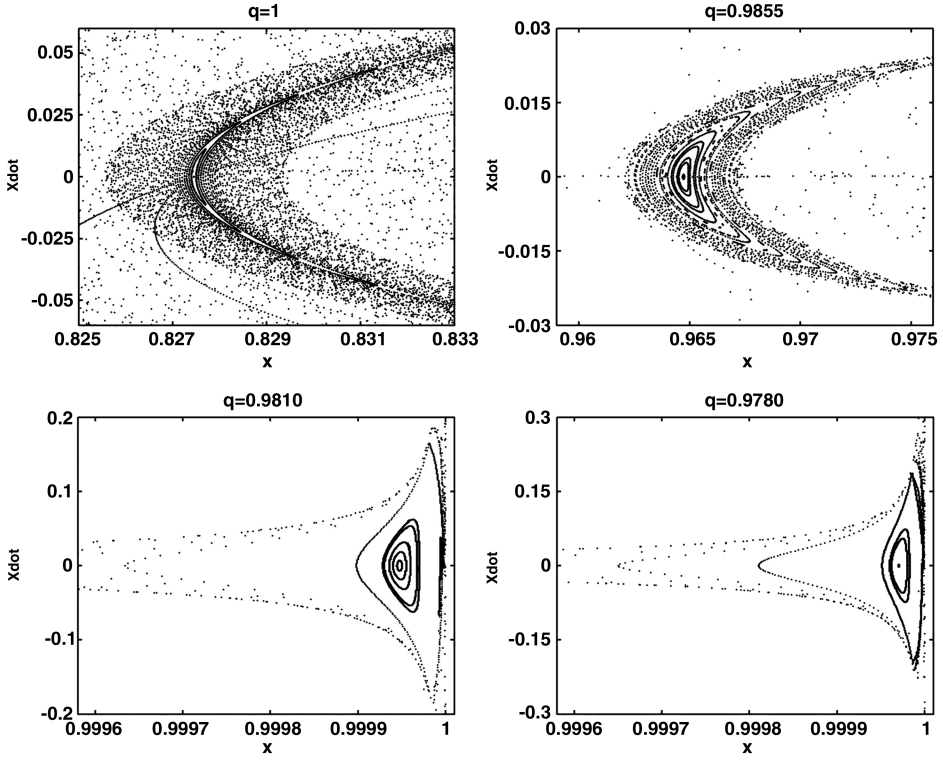

Fig. 10 PSS for Jacobi constant $C = 2.97$, with $q = 1, 0.9855, 0.9810$, and 0.9780.

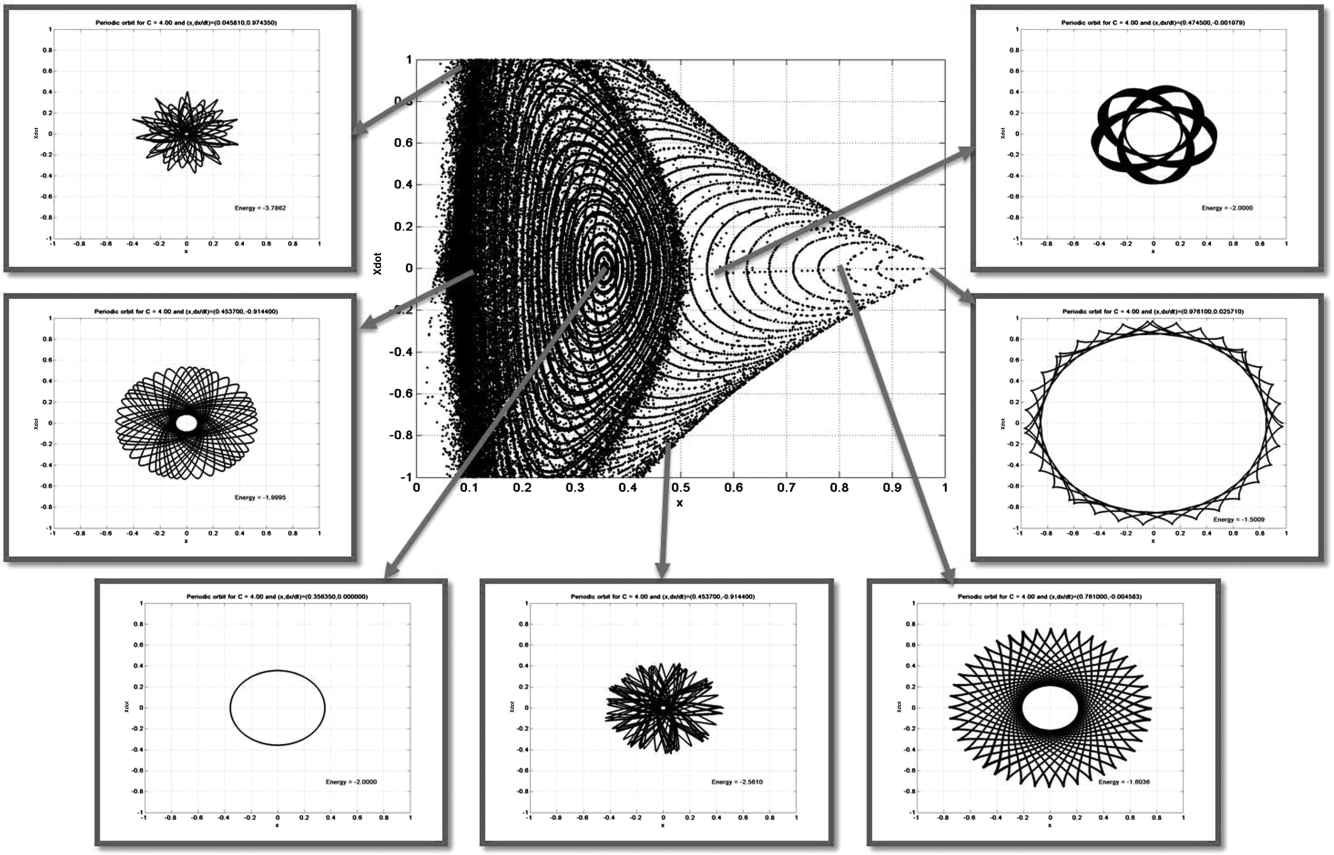

Fig. 12 Various orbits obtained from the PSS for $C = 4.0$ ($q = 1$).

maximum, after which it starts decreasing. From $C = 2.9996$ to 2.99993, the maximum amplitude of oscillation decreases uniformly and the KAM torus disappears at $C = 2.999933$. The islands reappear again and the stability increases, reaching a peak at $C = 2.99995$. Then the islands decrease uniformly until they disappear at $C = 3$. After that the islands reappear again and the width of KAM tori increases till $C = 3.00005$ and then it starts decreasing. The disappearance of the region of stability at two distinct values of Jacobi constant ($C = 2.999933$ and 3.0) is caused by the intersection of the central stable periodic orbit and an unstable periodic orbit usually lying at the three corners of the triangular stability region. For $C < 2.999933$, the quasi-periodic orbits oscillate about the periodic orbits in such a way that the farthest point from Mars, in the line of conjunction, is pericenter while for $2.999933 < C < 3.0$, the closest point to Mars is pericenter. Again for $C > 3.0$, the pericenter is the farthest point from Mars (Fig. 4). The variation in the width of the islands with C can be seen in Fig. 5. The transitions at $C = 2.999933$ and 3.0 are clearly seen in the zoomed version (where C varies from 2.9996 to 3.00003) of the same figure. The value of $\Delta x = 10^{-5}$ can be taken as error bar for the determination of the width of the KAM tori in this case. Some of the Mars-centered retrograde periodic orbits identified from PSS for different values of C are given in Fig. 6. It may be noted that the shape of the orbits transforms from kidney-bean shaped to near-circular and their size decreases with the increase in C. Further, as C varies from 1.55 to 3.015, the diameter of the periodic orbits decreases from 438,000,000 to 9800 km. Figure 7 gives a comparison of the size and shape of the periodic orbits for $C = 3.0007$ to 3.015. As C increases further, the orbits become smaller.

It is found that for $C = 3$, $(x, \dot{x}) = (0.9956, 0)$ is the point at which the island disappears. It is seen that at this point initially the orbit remains around Mars and as time progresses; it transforms into an orbit around the sun. Figure 8 shows the variation in the x-coordinate of the trajectory with time, and snapshots of the trajectory at different time instances.

B. Evolution of Mars-Centered Orbits with Radiation Pressure

It is observed that with increase in radiation pressure, the KAM tori move towards Mars. Figure 9 depicts the center of KAM tori containing the Mars-centered orbits with increase in radiation pressure for $C = 2.95$, 2.96, 2.97 and 2.98. Figure 10 provides the PSS for $C = 2.97$ when $q = 1$, 0.9855, 0.9810 and 0.9780. It is observed that the center of the KAM tori moves towards Mars and its width decreases with the increase in radiation pressure. For $C = 2.97$, Mars-centered periodic orbits are plotted in Fig. 11. It is seen that the size of the orbits decreases as radiation pressure increases. It may be seen from Figs. 7 and 11 that the nature of variation in the orbits is different with change in C and q.

C. Evolution of Sun-Centered Orbits Without Radiation Pressure

The KAM tori contain a number of sun-centered direct periodic orbits. Figure 12 provides the PSS for $C = 4$ along with some of the orbits. The largest KAM torus containing sun-centered orbit moves towards sun (Fig. 13a) and their size decreases (Fig. 13b) as C increases. The accuracy in the width of KAM tori is of the order of 10^{-3}, which is the value of Δx used for the generation of PSS for C lying between 3.05 and 7. Some of the periodic orbits obtained for $C = 2.97$ are shown in Fig. 14. They are arranged according to their location in the PSS. The fourth orbit in the second row of Fig. 14 is retrograde Mars-centered orbit. It can be seen that the loops in the sun-centered orbits between the sun and the Mars-centered orbit increase from two to eight and the loops are outward. While in the sun-centered orbits lying between the Mars-centered orbit and Mars, the number of loops decreases from five to one and the loops are inward. Figure 15 provides the evolution of a typical one-loop sun-centered orbit for the value of C from 1.6 to 2.97. As C increases, the size of the orbits decreases, while the shape of the loop changes from a kidney-bean shape to elliptical and its size decreases. Figure 16 provides the evolution of a two-loop orbit for the value of C from 2.4 to 3.17. It is noted that the size of the orbit along the y-axis decreases as C increases.

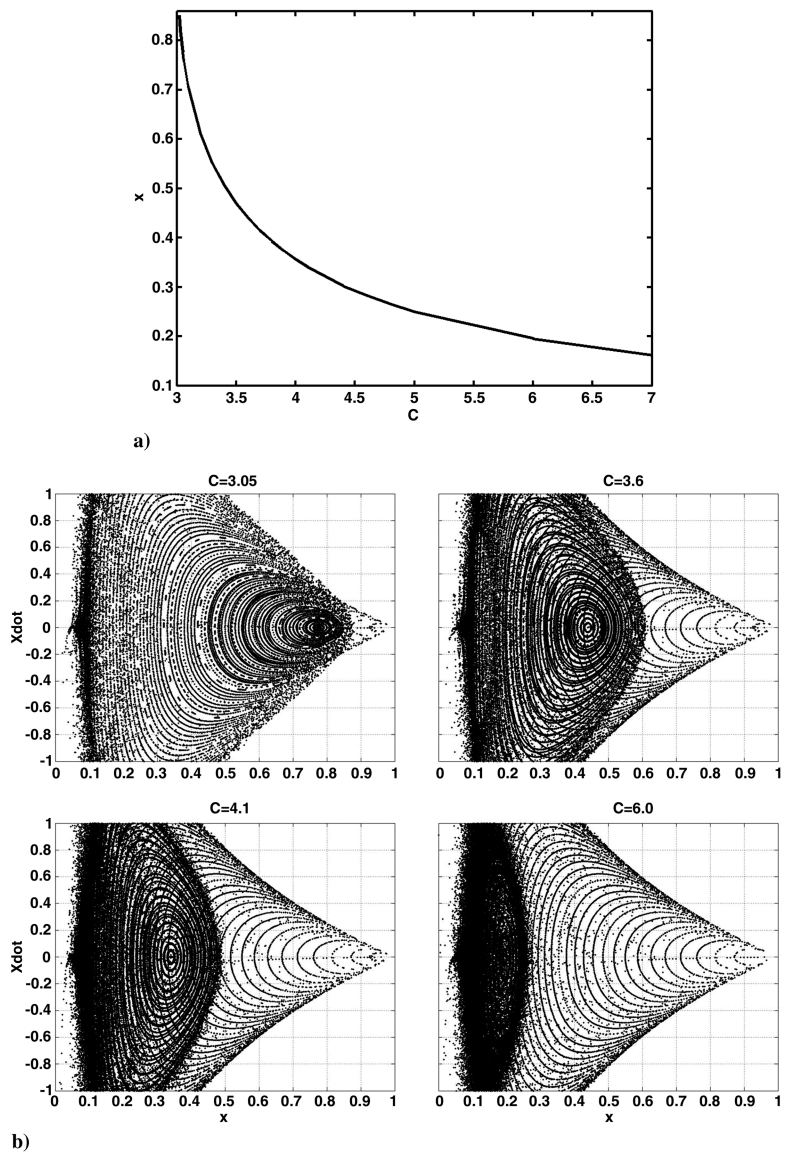

Fig. 13 KAM tori and PSS for sun-centered periodic orbits without radiation pressure: a) location of center of largest KAM tori containing the sun-centered periodic orbits as a function of the Jacobi constant C ($q = 1$) and b) PSS for $C = 3.05$, 3.6, 4.1, and 6.0.

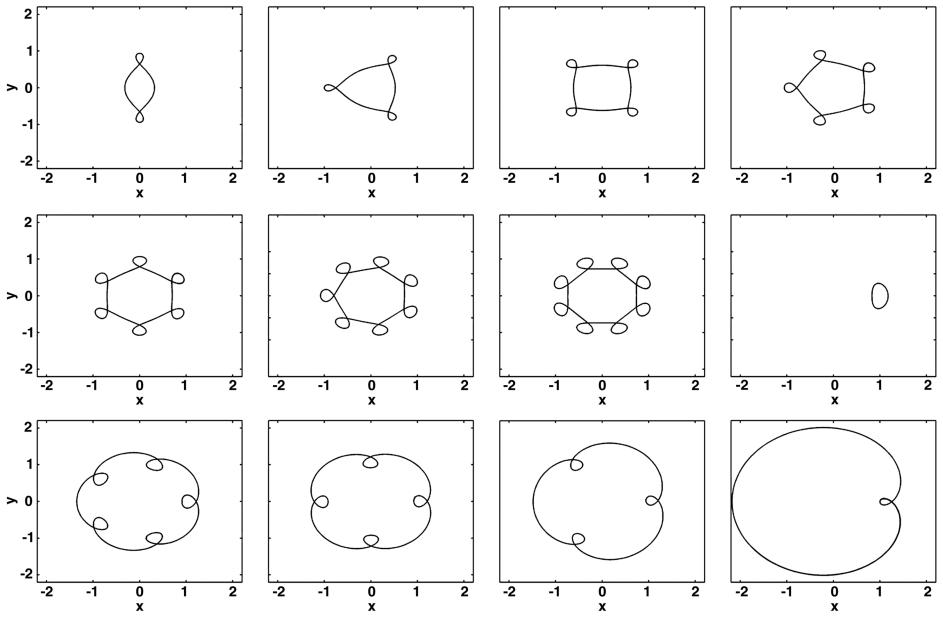

Fig. 14 Some orbits for $C = 2.97$ and $q = 1$. Orbits are arranged in ascending order of their location in the PSS.

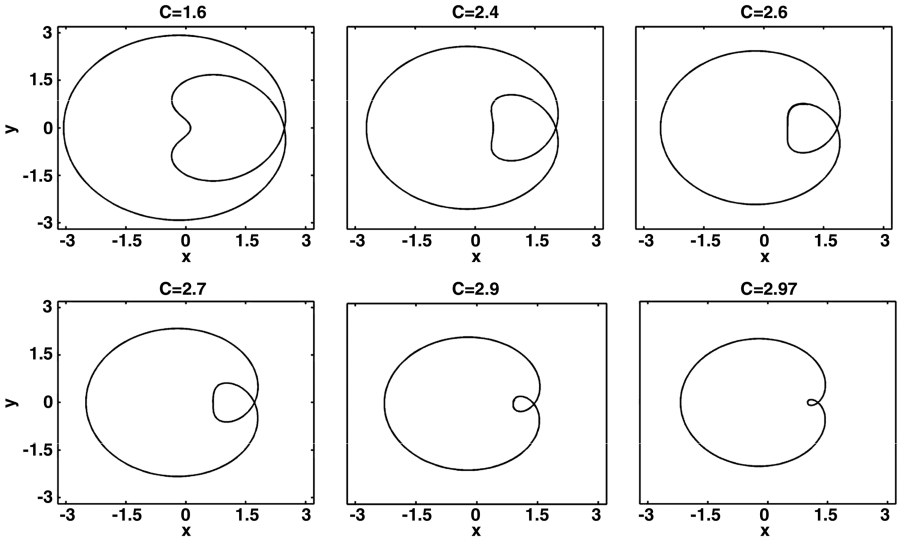

Fig. 15 Variation in one-loop orbits with Jacobi constant C ($q = 1$).

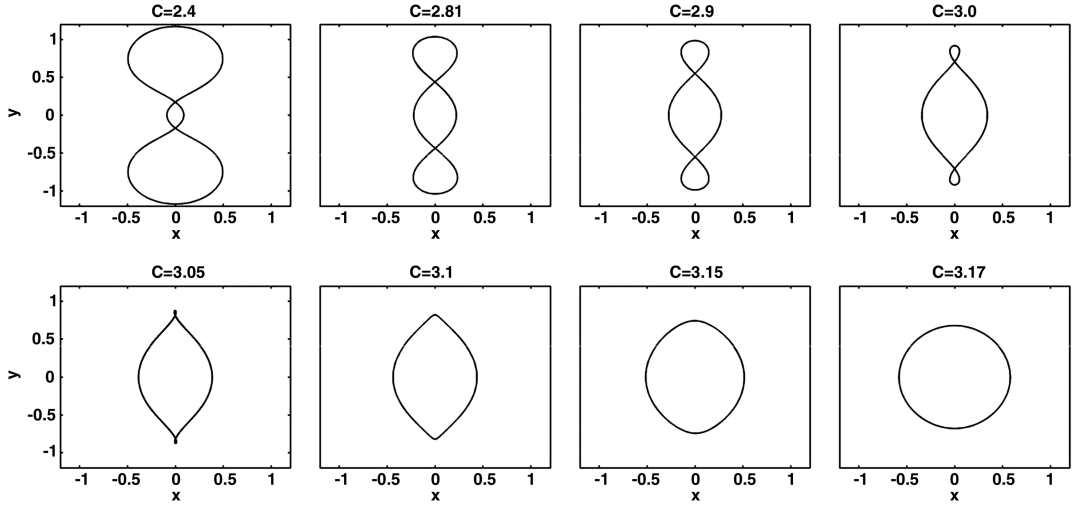

Fig. 16 Change in two-loop orbits with Jacobi constant C ($q = 1$).

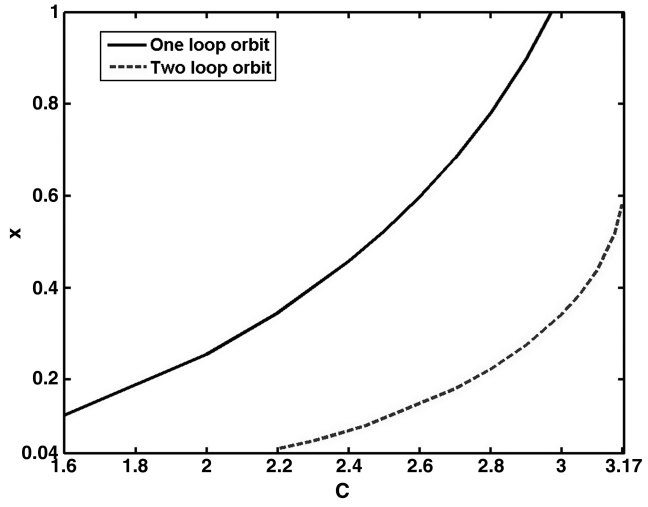

Fig. 17 Location of the one-loop and two-loop orbits in the PSS as a function of the Jacobi constant C ($q = 1$).

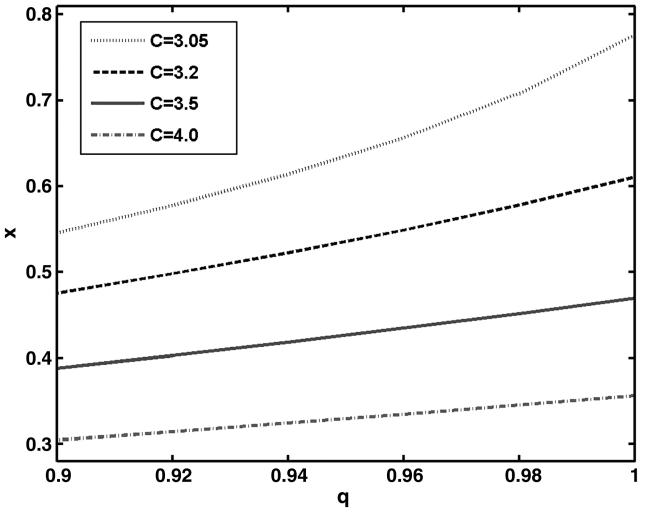

Fig. 18 Location of center of the biggest KAM tori containing the sun-centered periodic orbits as a function of solar radiation pressure (q).

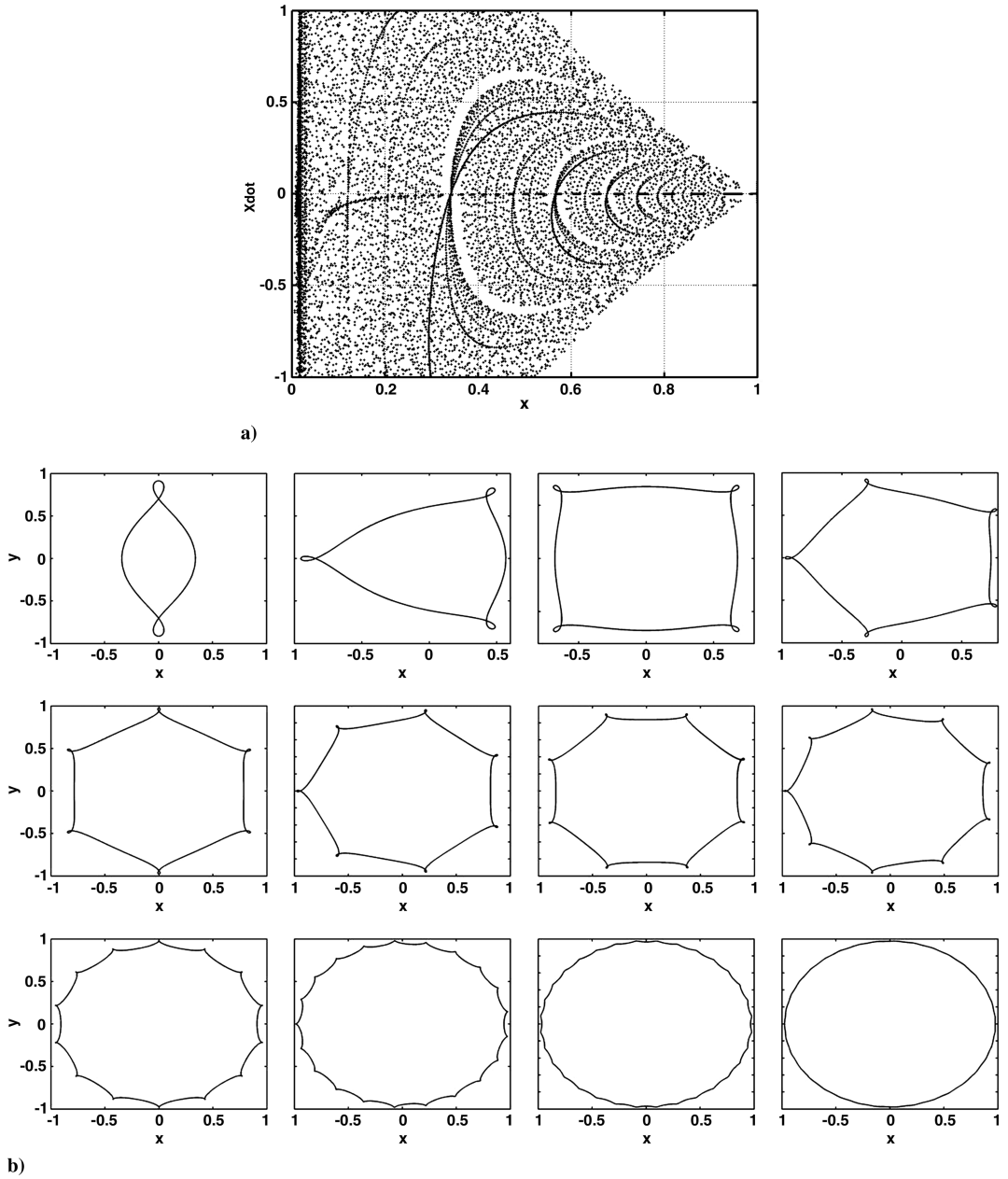

Fig. 19 PSS and sun-centered periodic orbits with radiation pressure: a) PSS for Jacobi constant $C = 2.97$ and $q = 0.9849$ and b) direct sun-centered periodic orbits for $C = 2.97$ and $q = 0.9849$ arranged according to their location on the PSS.

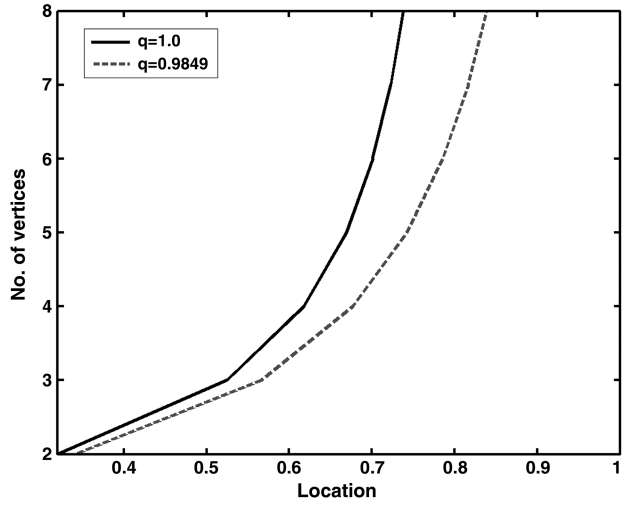

Fig. 20 Location of sun-centered direct periodic orbits on the PSS and the number of their vertices for $C = 2.97$ for $q = 1$ and $q = 0.9849$.

The two loops also decrease in size as C increases and eventually they vanish and near-circular orbit is obtained at $C = 3.17$. The location of one-looped and two-looped orbits in the PSS, as a function of C is given in Fig. 17.

D. Evolution of Sun-Centered Orbits with Radiation Pressure

Figure 18 provides the center of the largest KAM tori containing sun-centered orbits as function of q for different values of C. It is observed that only in this case the KAM tori move towards the sun as q decreases (solar radiation pressure increases). Large number of sun-centered periodic orbits was generated for different values of C and q. The orbits were found to be direct. As a typical case, PSS and periodic orbits for $C = 2.97$ with $q = 0.9849$ are presented in Figs. 19a and 19b, respectively. More than 74 periodic orbits are found. Out of these orbits, only one with initial $x = 0.99795$ is found to be an orbit around Mars, which is retrograde. It may be noted that only the orbit which is contained in the largest torus moves towards sun with increase in radiation pressure; whereas other orbits move towards Mars with increase in radiation pressure. Orbits with

Table 1 Typical orbits for $C = 2.97$ and $q = 0.9849$

No. of loops in the main orbit (orbits given in Fig. 19b)	No. of orbits on either side of the main orbit	No. of loops in the secondary orbits which lie between the sun and the main orbit	No. of loops in the secondary orbits which lie between the main orbit and Mars	Difference in number of loops between two consecutive secondary orbits
2	6	13, 11, 9, 7, 5, 3	13, 11, 9, 7, 5, 3	2
3	5	23, 20, 17, 14, 11	22, 19, 16, 13, 10	3
4	4	19, 15, 11, 7	17, 13, 9, 5	4
5	3	19, 14, 9	16, 11, 6	5
6	2	17, 11	13, 7	6

outward loops starting from two loops to 35 loops, some of them are shown in Fig. 19b, are obtained before the Mars-centered orbit appears. As the number of loops increases, the size of loops decreases. Figure 20 gives the number of vertices/loops present in these orbits and their location on PSS for $C = 2.97$ and $q = 1$, 0.9849. Some interesting observations are made. A number of orbits with different number of outward loops exist on either side of the main orbits (orbits which are shown in Fig. 19b), which also have outward loops. A definite trend in noticed in the number of loops and the difference in the number of loops between two consecutive orbits. For example, on either side of the main orbit with two loops, there are six orbits with 13, 11, 9, 7, 5 and 3 loops (difference of two loops between two consecutive orbits). It is interesting to note that these orbits are nearly equidistant from the two-looped main orbit (the first orbit in Fig. 19b). Similarly the main orbit with three loops (second orbit in Fig. 19b) is surrounded by five secondary orbits on both sides and the difference between the numbers of loops of two consecutive secondary orbits is three. Similar details of this and other main orbits containing two to six loops are provided in Table 1.

IV. Conclusions

The technique of PSS has been used to study the evolution of the sun-centered and the Mars-centered periodic orbits in the sun–Mars system. It is observed that only one Mars-centered orbit exist for a Jacobi constant C keeping radiation pressure constant, and this orbit shrinks in size with increase in C. It is also noted that there is a kind of separatrix between different types of quasi-periodic orbits around the Mars-centered periodic orbits at values of Jacobi constant equal to 2.999933 and 3. A number of sun-centered direct periodic orbits are obtained and an interesting symmetry among these orbits has been shown. The effect of radiation pressure due to the more massive primary (sun) on these orbits is studied. It is observed that as radiation pressure increases the largest KAM tori containing the sun-centered periodic orbits move towards the sun while tori containing other sun-centered orbits and the Mars-centered orbit move towards Mars. Some interesting results for Jacobi constant $C = 2.97$ and $q = 0.9849$ are highlighted. Since the increase in radiation pressure brings the Mars-centered orbit closer to Mars, it could be helpful for mission design, as with lesser energy closer orbits around Mars could be planned by increasing the radiation pressure.

Acknowledgments

The authors are thankful to the Associate Editor, Robert Melton, and the reviewer for their constructive comments, which helped in bringing this Note to the present form.

References

[1] Dutt, P., and Sharma, R. K., "Analysis of Periodic and Quasi-Periodic Orbits in the Earth–Moon System," *Journal of Guidance, Control, and Dynamics*, Vol. 33, No. 3, May–June 2010, pp. 1010–1017. doi:10.2514/1.46400

[2] Poynting, J. H., "Radiation in the Solar System: Its Effect on Temperature and its Pressure on Small Bodies," *Philosophical Transactions of the Royal Society of London. Series A, Physical Sciences and Engineering*, Vol. 202, 1904, pp. 525–552. doi: 10.1098/rsta.1904.0012

[3] Robertson, H. P., "Dynamical Effects of Radiation in the Solar System," *Monthly Notices of the Royal Astronomical Society*, Vol. 97, April 1937, pp. 423–438.

[4] Radzievskii, V. V., "The Restricted Problem of Three Bodies Taking Account of Light Pressure," *Akademii Nauk USSR, Astronomicheskii Zhurnal*, Vol. 27, No. 5, 1950, pp. 250–256.

[5] Chernikov, Y. A., "The Photogravitational Restricted Problem of Three Bodies," *Astronomicheskii Zhurnal*, Vol. 47, Feb. 1970, pp. 217–223 (in Russian).

[6] Manju and Choudhary, R. K., "On the Stability of Triangular Libration Points Taking into Account the Light Pressure for the Circular Restricted Problem of Three Bodies," *Celestial Mechanics*, Vol. 36, No. 2, 1985, pp. 165–190. doi:10.1007/BF01230650

[7] Kumar, V., and Choudhary, R. K., "On the Stability of the Triangular Libration Points for the Photo Gravitational Circular Restricted Problem of Three Bodies when Both of the Attracting Bodies are Radiating as Well," *Celestial Mechanics*, Vol. 40, No. 2, 1987, pp. 155–170. doi:10.1007/BF01230257

[8] Lukyanov, L. G., "On the Family of the Libration Points in the Restricted Photogravitational Three-Body Problem," *Astronomicheskii Zhurnal*, Vol. 65, March–April 1988, pp. 422–432.

[9] Kalvouridis, T. J., Arribas, M., and Elipe, A., "Parametric Evolution of Periodic Orbits in the Restricted Four-Body Problem with Radiation Pressure," *Planetary and Space Science*, Vol. 55, No. 4, 2007, pp. 475–493. doi:10.1016/j.pss.2006.07.005

[10] Sharma, R. K., "The Linear Stability of Libration Points of the Photogravitational Restricted Three-Body Problem when the Massive Primary is an Oblate Spheroid," *Sun and Planetary System: Proceedings of the Sixth European Regional Meeting in Astronomy*, Reidel, Dordrecht, The Netherlands, 1982, pp. 435–436.

[11] Sharma, R. K., "The Linear Stability of Libration Points of the Photogravitational Restricted Three-Body Problem when the Smaller Primary is an Oblate Spheroid," *Astrophysics and Space Science*, Vol. 135, No. 2, 1987, pp. 271–281. doi:10.1007/BF00641562

[12] Sharma, R. S., and Ishwar, B., "Critical Mass Value and Secular Solutions of the Photo Gravitational Restricted Three-Body Problem when the Smaller Primary is an Oblate Spheroid and Bigger a Source of Radiation," *Proceedings of the Workshop on Space Dynamics and Celestial Mechanics*, edited by K. B. Bhatnagar and B. Ishwar, BRA Bihar Univ., India, 18–22 Sept. 1995, pp. 31–39.

[13] Bhatnagar, K. B., and Chawla, J. M., "A study of the Lagrangian points in Photogravitational Restricted Three-Body Problem," *Indian Journal of Pure and Applied Mathematics*, Vol. 10, No. 11, Nov. 1979, pp. 1443–1451.

[14] Kalantonis, V. S., Perdios, E. A., and Ragos, O., "Asymptotic and Periodic Orbits Around L3 in Photogravitational Restricted Three-Body Problem," *Astrophysics and Space Science*, Vol. 301, Nos. 1–4, 2006, pp. 157–165. doi:10.1007/s10509-006-1305-0

[15] Kunitsyn, A. L., and Perezhogin, A. A., "On the Stability of Triangular Libration Points of the Photogravitational Restricted Circular Three-Body Problem," *Celestial Mechanics*, Vol. 18, No. 4, 1978, pp. 395–408.

[16] Kunitsyn, A. L., and Tureshbaev, A. T., "On the Collinear Libration Points in the Photogravitational Three-Body Problem," *Celestial Mechanics*, Vol. 35, No. 2, 1985, pp. 105–112. doi:10.1007/BF01227664

[17] Papadakis, K. E., "Asymptotic Orbits at the Triangular Equilibria in the Photogravitational Restricted Three-Body Problem," *Astrophysics and Space Science*, Vol. 305, No. 1, 2006, pp. 57–66. doi:10.1007/s10509-006-9043-x

[18] Ragos, O., and Zagouras, C. G., "Periodic Solutions About the 'Out Of Plane' Equilibrium Points in the Photogravitational Restricted Three-Body Problem," *Celestial Mechanics*, Vol. 44, Nos. 1–2, 1988, pp. 135–154.

doi:10.1007/BF01230711
[19] Ragos, O., and Zagouras, C. G., "On the Existence of the 'Out Of Plane' Equilibrium Points in the Photogravitational Restricted Three-Body Problem," *Astrophysics and Space Science*, Vol. 209, No. 2, 1993, pp. 267–271.
doi:10.1007/BF00627446
[20] Schuerman, D. W., "The Effect of Radiation Pressure on the Restricted Three-Body Problem," *Solid Particles in the Solar System*, edited by I. Halliday and B. A. McIntosh, Springer, Berlin, 1980, pp. 285–288.
[21] Abdul Raheem, A. R., and Singh, J., "Combined Effects of Perturbations, Radiation and Oblateness on the Stability of Equilibrium Points in the Restricted Three-Body Problem," *Astronomical Journal*, Vol. 131, No. 3, 2006, pp. 1880–1885.
doi:10.1086/499300
[22] Namboodiri, N. I. V., Reddy, D. S., and Sharma, R. K., "Effect of Oblateness and Radiation Pressure on Angular Frequencies at Collinear Points," *Astrophysics and Space Science*, Vol. 318, Nos. 3–4, 2008, pp. 161–168.
doi:10.1007/s10509-008-9934-0
[23] Markellos, V. V., Perdios, E., and Papadakis, K., "The Stability of Inner Collinear Equilibrium Points in the Photogravitational Elliptic Restricted Problem," *Astrophysics and Space Science*, Vol. 199, No. 1, 1993, pp. 139–146.
doi:10.1007/BF00612984
[24] Das, M. K., Narang, P., Mahajan, S., and Yuasa, M., "Effect of Radiation on the Stability of a Retrograde Particle Orbit in Different Stellar Systems," *Planetary and Space Science*, Vol. 57, No. 7, June 2009, pp. 836–845.
doi:10.1016/j.pss.2009.02.007
[25] Das, M. K., Narang, P., Mahajan, S., and Yuasa, M., "On out of Plane Equilibrium Points in Photogravitational Restricted Three-Body Problem," *Journal of Astrophysics and Astronomy*, Vol. 30, Nos. 3–4, 2009, pp. 177–185.
doi:10.1007/s12036-009-0009-6
[26] Szebehely, V., *Theory of Orbits*, Academic Press, New York, 1967, pp. 7–15.
[27] Broucke, R. A., "Periodic Orbits in the Restricted Three-Body Problem with Earth–Moon Masses," Jet Propulsion Lab. TR 32-1168, 1968.
[28] Markellos, V. V., "Numerical Investigation of the Planar Restricted Three-Body Problem. II: Regions of Stability for Retrograde Satellites of Jupiter as Determined by Periodic Orbits of the Second Generation," *Celestial Mechanics*, Vol. 10, No. 1, 1974, pp. 87–134.
doi:10.1007/BF01261880
[29] Gonczi, R., and Froeschle, C., "The Lyapunov Characteristic Exponents as Indicators of Stochasticity in the Restricted Three-Body Problem," *Celestial Mechanics*, Vol. 25, No. 3, 1981, pp. 271–280.
doi:10.1007/BF01228964
[30] Cielaszyk, D., and Wie, B., "New Approach to Halo Orbit Determination and Control," *Journal of Guidance, Control, and Dynamics*, Vol. 19, No. 2, 1996, pp. 266–273.
doi:10.2514/3.21614
[31] Papadakis, K. E., "Families of Periodic Orbits in the Photogravitational Three-Body Problem," *Astrophysics and Space Science*, Vol. 245, No. 1, 1996, pp. 1–13.
doi:10.1007/BF00637799
[32] Henon, M., *Generating Families in the Restricted Three Body Problem*, Springer, New York, 1997.
[33] Perdios, E. A., Kalantonis, V. S., and Vrahatis, M. N., "Efficient Method for Computing with Certainty Periodic Orbits on a Surface of Section," *Celestial Mechanics and Dynamical Astronomy*, Vol. 84, No. 3, 2002, pp. 231–244.
doi:10.1023/A:1020338609583
[34] Tsirogiannis, G. A., Perdios, E. A., and Markellos, V. V., "Global Data Clustering for Periodic Orbits," *Dynamics of Celestial Bodies: Proceedings of the 2008 International Conference in Honor of John D. Hadjidemetriou*, Special Issue, 2009, pp. 185–188.
[35] Russell, R., "Global Search for Planar and Three-Dimensional Periodic Orbits near Europa," AAS/AIAA Astrodynamics Specialist Conference, Lake Tahoe, CA, American Astronomical Society Paper 05-290, 7–11 Aug. 2005.
[36] Viswanath, D., "The Lindstedt–Poincaré Technique as an Algorithm for Computing Periodic Orbits," *SIAM Review*, Vol. 43, No. 3, 2001, pp. 478–495.
doi:10.1137/S0036144500375292
[37] Deprit, A., and Rom, A., "Poincaré's Continuation by Computer," *AIAA Journal*, Vol. 6, No. 7, 1968, pp. 1234–1239.
doi:10.2514/3.4727
[38] Williams, P., "Direct Numerical Computation of Periodic Orbits and their Stability," *Journal of Spacecraft and Rockets*, Vol. 43, No. 5, 2006, pp. 1143–1146.
doi:10.2514/1.20930
[39] Gilbout, V. M., and Scheeres, D. J., "Periodic Orbits from Generating Functions," American Astronomical Society Paper 03-566, 2003, pp. 1029–1048.
[40] Winter, O. C., "The Stability Evolution of a Family of Simply Periodic Lunar Orbits," *Planetary and Space Science*, Vol. 48, No. 1, 2000, pp. 23–28.
doi:10.1016/S0032-0633(99)00082-3